

RSC Advances



This is an *Accepted Manuscript*, which has been through the Royal Society of Chemistry peer review process and has been accepted for publication.

Accepted Manuscripts are published online shortly after acceptance, before technical editing, formatting and proof reading. Using this free service, authors can make their results available to the community, in citable form, before we publish the edited article. This *Accepted Manuscript* will be replaced by the edited, formatted and paginated article as soon as this is available.

You can find more information about *Accepted Manuscripts* in the [Information for Authors](#).

Please note that technical editing may introduce minor changes to the text and/or graphics, which may alter content. The journal's standard [Terms & Conditions](#) and the [Ethical guidelines](#) still apply. In no event shall the Royal Society of Chemistry be held responsible for any errors or omissions in this *Accepted Manuscript* or any consequences arising from the use of any information it contains.

**A series of mixed-ligand 2D and 3D coordination polymers
assembled from a novel multifunctional pyridine-tricarboxylate
building block: hydrothermal syntheses, structural and
topological diversity, and magnetic and luminescent properties†**

Jin-Zhong Gu,^{*a} Yan-Hui Cui,^a Jiang Wu,^a and Alexander M. Kirillov^b

^a *Key Laboratory of Nonferrous Metal Chemistry and Resources Utilization of Gansu Province, College of Chemistry and Chemical Engineering, Lanzhou University, Lanzhou 730000, P. R. China*

^b *Centro de Química Estrutural, Complexo I, Instituto Superior Técnico, Universidade de Lisboa, Av. Rovisco Pais, 1049-001, Lisbon, Portugal*

* Corresponding author. Fax: +86 931 8915196. *E-mail address:* gujzh@lzu.edu.cn (J.-Z. Gu).

Abstract

A series of novel mixed-ligand coordination polymers, namely, $\{[\text{Cd}_2(\mu_4\text{-L})(\mu_3\text{-OH})(\text{phen})_2]\cdot 2\text{H}_2\text{O}\}_n$ (**1**), $\{[\text{Mn}_3(\mu_5\text{-L})_2(\text{phen})_2(\text{H}_2\text{O})]\cdot \text{H}_2\text{O}\}_n$ (**2**), $[\text{Cd}_2(\mu_3\text{-L})(\text{H}_2\text{biim})_2(\mu_2\text{-Hbiim})]_n$ (**3**), $\{[\text{Pb}_2(\mu_4\text{-L})(\mu_4\text{-bpdc})_{0.5}(\text{phen})_2]\cdot \text{H}_2\text{O}\}_n$ (**4**), $[\text{Cd}_2(\mu_5\text{-L})(\mu_2\text{-bpdc})_{0.5}(\text{phen})_2]_n$ (**5**), and $[\text{Zn}_2(\mu_4\text{-L})(\mu_2\text{-bpdc})_{0.5}(\text{py})_2]_n$ (**6**), was hydrothermally synthesized using 4-(5-carboxypyridin-2-yl)isophthalic acid (H_3L) as a new and virtually unexplored multifunctional pyridine-tricarboxylate building block, along with various auxiliary ligands {phen = 1,10-phenanthroline, H_2biim = 2,2'-biimidazole, H_2bpdc = 4,4'-biphenyldicarboxylic acid, and py = pyridine}. All the products **1–6** were characterized by IR spectroscopy, elemental, thermogravimetric, and single-crystal X-ray diffraction analyses. Compounds **1**, **3**, and **5** reveal the 2D metal-organic layers with the **kgd**, **fes**, and **3,4,5L5** topology, respectively, whereas the metal-organic frameworks (MOFs) **2**, **4**, and **6** disclose the 3D underlying nets with the unique (**2**, **4**) or **ins** (**6**) topology. The results indicate that the nature of metal(II) ion and type of auxiliary ligand play a significant role in determining the dimensionality, topology and other structural features of the obtained products. Luminescent (for **1** and **3–6**) and magnetic (for **2**) properties were studied and discussed.

Keywords: 4-(5-carboxypyridin-2-yl)isophthalic acid, coordination polymers, photoluminescence, magnetism, crystal engineering.

1. Introduction

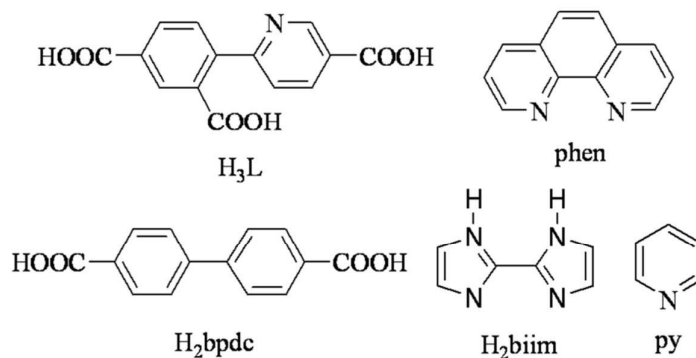
The research on coordination polymers has recently attracted very high attention due to their intriguing architectures and variety of applications.¹ However, it is usually difficult to control the structural and functional characteristics of coordination polymers during the self-assembly syntheses, because many factors can affect the result, such as the coordination geometry of metal ions, connectivity of organic building blocks, stoichiometry, reaction conditions (temperatures, solvents, pH values), and presence of auxiliary ligands.² A rather effective and facile approach to achieve better synthetic predictability consists of the appropriate choice of the organic bridging ligands bearing modifiable backbones, along with the selection of metal centers possessing various coordination preferences. A considerable number of aromatic polycarboxylic acids including N-heterocyclic derivatives has been extensively applied in crystal engineering of coordination polymers.³ Among such ligands, flexible biphenyl polycarboxylic acids have attracted a recent interest due to the presence of two phenyl rings that can be rotated around the C–C single bond, thus facilitating the binding to metal cations. Besides, complete or partial deprotonation of such multicarboxylate blocks can induce the variation of coordination modes and allow the generation of structurally distinct metal-organic frameworks.⁴ Moreover, such ligands can act as H-bond acceptors and donors, depending upon the degree of deprotonation, thus providing an additional structural reinforcement.

Although a substantial number of coordination polymers incorporating various kinds of carboxylate ligands has been reported, the examples of compounds

constructed from a combination of two kinds of biphenyl carboxylate building blocks are barely known, mainly due to different solubility of such ligands, distinct charges and coordination modes, as well as competition with each other during the self-assembly syntheses. In fact, the effect of two different types of biphenyl carboxylate moieties on the structure of the resulting metal-organic framework remains poorly studied. A reaction containing multiple ligands can lead to a mixed-ligand phase, a biphasic mixture, or a pure sample wherein only one ligand is incorporated whereas another one remains in solution. The process can become even more challenging when there is an extra auxiliary ligand apart from two biphenyl carboxylate building blocks. Since it is still very difficult to predict the result of the self-assembly syntheses in these multi-ligand reaction mixtures, a prior examination of the compounds containing several ligands from the same broad family will enhance the understanding of such systems.⁵ Apart from multifunctional carboxylate ligands, 1,10-phenanthroline (phen), 2,2'-biimidazole (H₂biim) and pyridine (py) are frequently applied as simple N-donor auxiliary ligands to tune the coordination environment of metal centers and stabilize the structures of coordination polymers, namely, due to $\pi\cdots\pi$ stacking and H-bonding interactions.^{4a,4b,6-11}

Taking into consideration the above-mentioned points, the main objectives of the present study were the following: (1) to design a novel multifunctional polycarboxylate building block for the synthesis of coordination polymers or metal-organic frameworks, (2) to prepare unusual mixed-ligand coordination compounds that would incorporate two different types of biphenyl carboxylate

building blocks, and (3) to fully characterize the obtained compounds, explore their structural and topological features and investigate functional properties. Thus, we have attempted a series of hydrothermal self-assembly reactions between different metal(II) chlorides ($M = \text{Cd}, \text{Mn}, \text{Pb}$ and Zn) and 4-(5-carboxypyridin-2-yl)isophthalic acid (H_3L) as a new principal building block, along with optional 4,4'-biphenyldicarboxylic acid (H_2bpdc) as a secondary biphenyl carboxylate block, and also in the presence of an auxiliary ligand selected from 1,10-phenanthroline (phen), 2,2'-biimidazole (H_2biim), or pyridine (py). The present study thus reports the syntheses, full characterization, structural and topological features, as well as luminescent or magnetic properties of six new coordination polymers, namely, $\{[\text{Cd}_2(\mu_4\text{-L})(\mu_3\text{-OH})(\text{phen})_2] \cdot 2\text{H}_2\text{O}\}_n$ (1), $\{[\text{Mn}_3(\mu_5\text{-L})_2(\text{phen})_2(\text{H}_2\text{O})] \cdot \text{H}_2\text{O}\}_n$ (2), $[\text{Cd}_2(\mu_3\text{-L})(\text{H}_2\text{biim})_2(\mu_2\text{-Hbiim})]_n$ (3), $\{[\text{Pb}_2(\mu_4\text{-L})(\mu_4\text{-bpdc})_{0.5}(\text{phen})_2] \cdot \text{H}_2\text{O}\}_n$ (4), $[\text{Cd}_2(\mu_5\text{-L})(\mu_2\text{-bpdc})_{0.5}(\text{phen})_2]_n$ (5), and $[\text{Zn}_2(\mu_4\text{-L})(\mu_2\text{-bpdc})_{0.5}(\text{py})_2]_n$ (6). To our knowledge, the obtained products represent the first structurally characterized examples of coordination compounds derived from H_3L , as attested by a search of the Cambridge Structural Database.



Scheme 1 Structural formulae of used building blocks.

2. Experimental

2.1 Materials and methods

All chemicals and solvents were of A.R. grade and used without further purification, except for H₃L that was synthesized by adapting a literature method.¹² ¹H NMR spectra were performed on a Bruker Advance III 400 spectrometer. Carbon, hydrogen and nitrogen contents were determined using an Elementar Vario EL elemental analyzer. IR spectra were recorded using KBr pellets and a Bruker EQUINOX 55 spectrometer. Thermogravimetric analyses (TGA) were performed under N₂ atmosphere with a heating rate of 10 °C/min on a LINSEIS STA PT1600 thermal analyzer. Powder X-ray diffraction patterns (PXRD) were determined with a Rigaku-Dmax 2400 diffractometer using Cu-K α radiation. Magnetic susceptibility data were collected in the 2–300 K temperature range with a Quantum Design SQUID Magnetometer MPMS XL-7 with a field of 0.1 T. A correction was made for the diamagnetic contribution prior to data analysis. Excitation and emission spectra were recorded at room temperature for the solid samples using an Edinburgh FLS920 fluorescence spectrometer.

2.2 Synthesis of 4-(5-carboxypyridin-2-yl)isophthalic acid (H₃L)

A mixture of ethyl 6-bromonicotinate (115.0 mg, 0.50 mmol) (a), 2,4-bis(ethoxycarbonyl)phenylboronic acid (143.0 mg, 0.55 mmol) (b), K₂CO₃ (210.0 mg, 1.5 mmol), Pd(OAc)₂ (56 mg, 0.025 mmol), and C₂H₅OH (50 mL) was stirred and refluxed for 10 h. After cooling to room temperature, the precipitate was filtered

off, and the filtrate was concentrated under reduced pressure. The obtained residue was purified by silica gel column chromatography with dichloromethane/ethyl acetate 36 : 1 to give diethyl 4-(5-(ethoxycarbonyl)pyridin-2-yl)isophthalate as a white solid. A suspension of diester in 1 M NaOH was stirred at 80 °C for 2 h. The solution was cooled with ice and acidified with HCl to pH = 2.5. The white precipitate was collected to give H₃L in 43% yield based on ethyl 6-bromonicotinate. Calcd for C₁₄H₉NO₆ (287.22): C 58.54, H 3.16, N 4.88%. Found: C 58.18, H 3.07, N 4.95%. IR (KBr, cm⁻¹): ν(COO) 1684 s. ¹H NMR (400 MHz, DMSO-*d*₆): δ 13.43 (s, 3H), δ 7.66-7.69 (m, 2H), δ 8.035 (d, *J* = 8.0 Hz, 1H), δ 8.186 (s, 1H), δ 8.237 (d, *J* = 8.0 Hz, 1H), δ 9.044 (s, 1H).

2.3 Synthesis of {[Cd₂(μ₄-L)(μ₃-OH)(phen)₂]·2H₂O}_n (**1**)

A mixture of CdCl₂·H₂O (60.3 mg, 0.3 mmol), H₃L (57.4 mg, 0.2 mmol), phen (60.0 mg, 0.3 mmol), NaOH (24.0 mg, 0.6 mmol), and H₂O (10 mL) was stirred at room temperature for 15 min, then sealed in a 25 mL Teflon-lined stainless steel vessel, and heated at 160 °C for 3 days, followed by cooling to room temperature at a rate of 10 °C h⁻¹. Colorless block-shaped crystals of **1** were isolated manually, and washed with distilled water and dried (yield 45% based on CdCl₂·H₂O). Anal. Calcd for C₃₈H₂₇Cd₂N₅O₉: C, 49.48; H, 2.95; N, 7.59. Found: C 49.28, H 3.06, N 7.34%. IR (KBr, cm⁻¹): 3457 w, 3055 w, 1588 s, 1516 m, 1429 m, 1373 s, 1145 m, 1102 w, 1025 w, 910 w, 861 m, 823 w, 785 m, 728 m, 702 w, 562 w.

2.4 Synthesis of $\{[\text{Mn}_3(\mu_5\text{-L})_2(\text{phen})_2(\text{H}_2\text{O})]\cdot\text{H}_2\text{O}\}_n$ (**2**)

Synthesis of **2** was similar to that of **1** except that $\text{CdCl}_2\cdot\text{H}_2\text{O}$ was replaced by $\text{MnCl}_2\cdot 4\text{H}_2\text{O}$ (60.0 mg, 0.3 mmol). Yellow block-shaped crystals of **2** were obtained (yield 60% based on $\text{MnCl}_2\cdot 4\text{H}_2\text{O}$). Anal. Calcd for $\text{C}_{52}\text{H}_{32}\text{Mn}_3\text{N}_6\text{O}_{14}$: C, 55.29; H, 2.86; N, 7.44. Found: C 55.08, H 2.92, N 7.26. IR (KBr, cm^{-1}): 3429 w, 3055 w, 1599 s, 1515 m, 1424 w, 1389 s, 1145m, 1102 w, 1026 w, 913 w, 848 m, 778 m, 730 m, 698 w, 563 w.

2.5 Synthesis of $[\text{Cd}_2(\mu_3\text{-L})(\text{H}_2\text{biim})_2(\mu_2\text{-Hbiim})]_n$ (**3**)

Synthesis of **3** was similar to that of **1** except that phen was replaced by H_2biim (39.2 mg, 0.30 mmol). Colorless block-shaped crystals of **3** were obtained (yield 35% based on $\text{CdCl}_2\cdot\text{H}_2\text{O}$). Anal. Calcd for $\text{C}_{32}\text{H}_{23}\text{Cd}_2\text{N}_{13}\text{O}_6$: C, 42.22; H, 2.55; N, 20.00. Found: C 41.98, H 2.65, N 20.27. IR (KBr, cm^{-1}): 1608 m, 1594 s, 1533 m, 1404 m, 1373 s, 1325 w, 1175 w, 1138 m, 1116 m, 1046 w, 992 w, 941 w, 852 w, 778 m, 762 m, 728 w, 711 w, 690 m, 556 w.

2.6 Synthesis of $\{[\text{Pb}_2(\mu_4\text{-L})(\mu_4\text{-bpdc})_{0.5}(\text{phen})_2]\cdot\text{H}_2\text{O}\}_n$ (**4**)

A mixture of PbCl_2 (111.2 mg, 0.4 mmol), H_3L (57.4 mg, 0.2 mmol), H_2bpdc (24.2 mg, 0.10 mmol), phen (80.0 mg, 0.4 mmol), NaOH (32.0 mg, 0.8 mmol), and H_2O (10 mL) was stirred at room temperature for 15 min, then sealed in a 25 mL Teflon-lined stainless steel vessel, and heated at 160 °C for 3 days, followed by cooling to room temperature at a rate of 10 °C h^{-1} . Colorless block-shaped crystals of **4** were isolated

manually, and washed with distilled water and dried (yield 65% based on PbCl_2). Anal. Calcd for $\text{C}_{45}\text{H}_{29}\text{Pb}_2\text{N}_5\text{O}_9$: C, 45.11; H, 2.44; N, 5.84. Found: C 45.57, H 2.56, N 6.06%. IR (KBr, cm^{-1}): 3436 w, 3053 w, 1579 s, 1530 m, 1424 m, 1370 s, 1145 m, 1098 w, 1025 w, 916 w, 859 m, 830 w, 782 m, 730 m, 708 m, 561 w.

2.6 Synthesis of $[\text{Cd}_2(\mu_5\text{-L})(\mu_2\text{-bpdc})_{0.5}(\text{phen})_2]_n$ (**5**)

Synthesis of **5** was similar to that of **4** except using $\text{CdCl}_2 \cdot \text{H}_2\text{O}$ (80.4 mg, 0.40 mmol) instead of PbCl_2 . Colorless block-shaped crystals of **5** were obtained (yield 60% based on $\text{CdCl}_2 \cdot \text{H}_2\text{O}$). Anal. Calcd for $\text{C}_{45}\text{H}_{27}\text{Cd}_2\text{N}_5\text{O}_8$: C, 54.56; H, 2.75; N, 7.07. Found: C 54.17, H 2.83, N 7.22. IR (KBr, cm^{-1}): 3408 w, 3060 w, 1583 s, 1537 m, 1428 w, 1372 s, 1140 m, 1101 w, 1024 w, 922 w, 848 m, 776 m, 726 m, 709 w, 640 w.

Synthesis of $[\text{Zn}_2(\mu_4\text{-L})(\mu_2\text{-bpdc})_{0.5}(\text{py})_2]_n$ (**6**)

A mixture of ZnCl_2 (54.5 mg, 0.4 mmol), H_3L (57.4 mg, 0.2 mmol), H_2bpdc (24.2 mg, 0.10 mmol), py (0.5 mL, 6.3 mmol), and H_2O (10 mL) was stirred at room temperature for 15 min, then sealed in a 25 mL Teflon-lined stainless steel vessel, and heated at 160 °C for 3 days, followed by cooling to room temperature at a rate of 10 °C h^{-1} . Colorless block-shaped crystals of **6** were isolated manually, and washed with distilled water and dried (yield 62% based on ZnCl_2). Anal. Calcd for $\text{C}_{31}\text{H}_{20}\text{Zn}_2\text{N}_3\text{O}_8$: C, 53.70; H, 2.91; N, 6.06. Found: C 53.37, H 3.09, N 6.25. IR (KBr, cm^{-1}): 1607 s, 1545 m, 1487 m, 1450 m, 1396 s, 1219 w, 1159 w, 1132 w, 1068 w, 1044 w, 1014 w, 852 m, 777 m, 724 w, 698 m, 636 w.

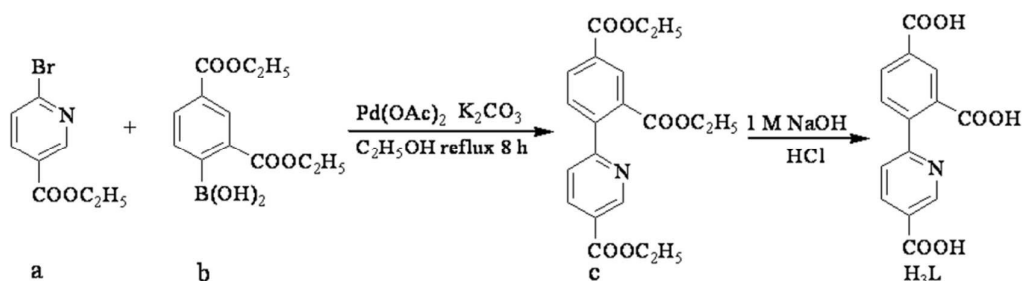
3. X-ray crystallography

The X-ray single-crystal data collection for compounds **1–6** was performed on an Agilent SuperNova diffractometer, using graphite-monochromated Mo K_α radiation ($\lambda = 0.71073 \text{ \AA}$). Semiempirical absorption corrections were applied using the SADABS program. The structures were solved by direct methods and refined by full-matrix least-squares on F^2 using the SHELXS-97 and SHELXL-97 programs.¹³ All non-hydrogen atoms were refined anisotropically by full-matrix least-squares methods on F^2 . The structures were solved using direct method, which yielded the positions of all non-hydrogen atoms. All the hydrogen atoms (except the ones bound to water molecules) were placed in calculated positions with fixed isotropic thermal parameters and included in structure factor calculations in the final stage of full-matrix least-squares refinement. The hydrogen atoms of water molecules were located by difference maps and constrained to ride on their parent O atoms. The final chemical formulas of **1–6** were calculated from SQUEEZE¹⁴ results combined with the data of TGA and elemental analysis. In compound **5**, four C atoms are disordered over two sites, that is, C41, C42, C44, C45 and C41', C42', C44', C45', with occupancy of 0.5. In addition, one O atom is also disordered over two sites, O2 and O2A, with occupancy of 0.6 and 0.4. Crystallographic data as well as details of data collection and refinement for **1–6** are summarized in Table 1, whereas selected bond lengths and angles are listed in Table S1 (ESI†). Hydrogen bonds in crystal packing for the compounds **1–6** are given in Table S2 (ESI†).

4. Results and discussion

4.1 Synthesis and characterization

The H₃L was synthesized by the Suzuki reaction.¹² The reaction route is given in Scheme 2.



Scheme 2 The synthetic route for H₃L ligand.

To explore 4-(5-carboxypyridin-2-yl)isophthalic acid as a building block toward crystal engineering of metal(II) (Cd, Mn, Pb, Zn) coordination polymers, we have attempted a number of hydrothermal reactions by treating different metal(II) chlorides with H₃L in the presence of some common auxiliary ligands or potential linkers, selected from 1,10-phenanthroline, 2,2'-biimidazole, pyridine, or 4,4'-biphenyldicarboxylic acid. The selection of metal(II) (Cd, Mn, Pb, and Zn) nodes has been governed by a good crystallization behavior of derived polycarboxylate coordination compounds, a particular suitability of such metal ions for the hydrothermal self-assembly synthesis and their coordination versatility,^{2b,2d,3b,3c,4a,4b} as well as interesting luminescent and/or magnetic properties of coordination polymers based on these metals.^{2b,2d,2f,3b,3d,3c,4a,4b,4g} Various stoichiometric ratios of reactants and combinations of auxiliary ligands have been tested, resulting in a few successful

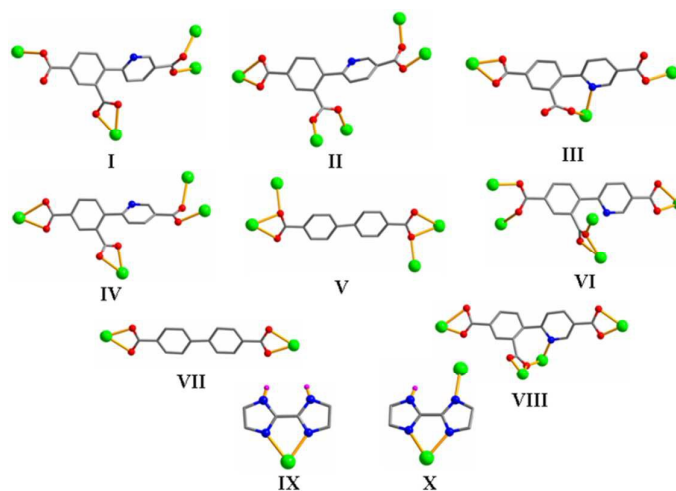
synthetic protocols that led to the isolation of single crystals suitable for X-ray diffraction. Compounds **1–3** were obtained by hydrothermal reactions using a mixture of the corresponding metal(II) chloride ($\text{CdCl}_2 \cdot \text{H}_2\text{O}$ or $\text{MnCl}_2 \cdot 4\text{H}_2\text{O}$) in H_2O with H_3L , phen or H_2biim , and NaOH in a 1.5 : 1 : 1.5 : 3 molar ratio, respectively. Coordination polymers **4** and **5** were synthesized in a similar way but using a mixture of PbCl_2 or $\text{CdCl}_2 \cdot \text{H}_2\text{O}$ with H_3L , H_2bpdc , phen, and NaOH as a base in a 4 : 2 : 1 : 4 : 8 molar ratio, respectively. Yet compound **6** was generated in an analogous manner by treating, in aqueous medium, ZnCl_2 with H_3L , H_2bpdc , and py taken in a 4 : 2 : 1 : 63 molar ratio, respectively. In the latter synthesis, pyridine served not only as an auxiliary ligand but also as a base. The structures of the obtained products were established by single crystal X-ray diffraction, analyzed from the topological viewpoint,^{15–18} and confirmed further by standard analytical methods.

4.2 Crystal structures

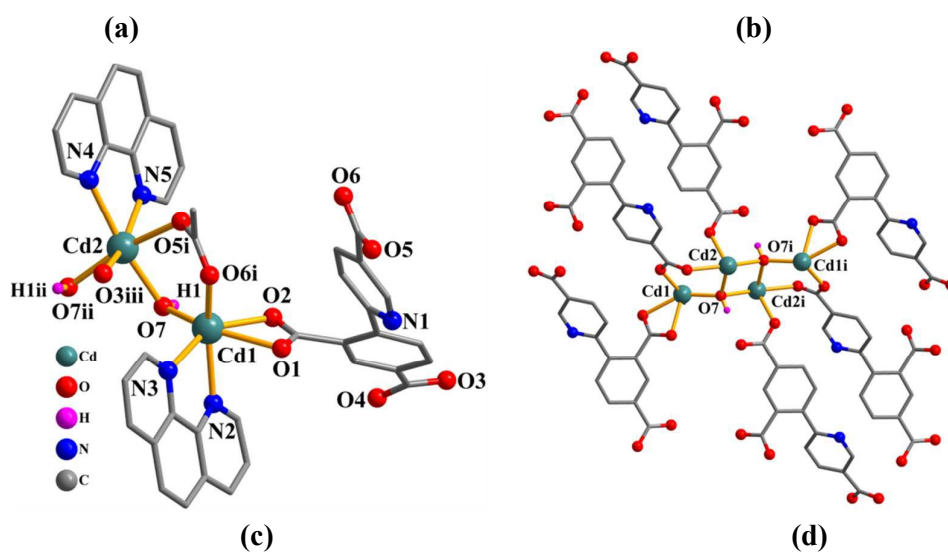
4.2.1 $\{[\text{Cd}_2(\mu_4\text{-L})(\mu_3\text{-OH})(\text{phen})_2] \cdot 2\text{H}_2\text{O}\}_n$ (**1**). The asymmetric unit of **1** contains two crystallographically unique Cd(II) ions, one $\mu_4\text{-L}^{3-}$ block, one $\mu_3\text{-OH}^-$ moiety, two terminal phen ligands, and two solvent water molecules. As depicted in Fig. 1a, both Cd1 and Cd2 atoms possess a distorted octahedral coordination environment. The Cd1 center is coordinated by three O atoms from two different $\mu_4\text{-L}^{3-}$ blocks, one O atom from $\mu_3\text{-OH}^-$ moiety and two N atoms from one phen ligand. The Cd2 center is bound by two O atoms from the two different $\mu_4\text{-L}^{3-}$ blocks, two O atoms from two $\mu_3\text{-OH}^-$ moieties, and two N atoms from phen ligand. The lengths of Cd–O bonds range from 2.195(2) to 2.458(3) Å, whereas the Cd–N bonds vary from 2.338(3) to 2.433(3) Å

(Table S1); these are within the normal values observed in various Cd(II) coordination compounds.^{2b,2h,3d,4a,5c,11,17} In **1**, the L³⁻ spacer exhibits a μ_4 -coordination mode (Scheme 3, mode I), in which the three carboxylate groups show different monodentate or bidentate modes. The dihedral angle between the pyridyl and phenyl rings in the L³⁻ is 42.51°. Two carboxylate groups from two different L³⁻ and two μ_3 -OH⁻ moieties bridge the four adjacent Cd(II) atoms to form a tetracadmium(II) unit (Fig. 1b), which is further connected by L³⁻ ligands to generate a 2D metal-organic layer (Fig. 1c). The 2D sheets are further extended into a 3D supramolecular framework by π - π stacking interactions between the adjacent pyridyl planes of phenyl ligands (Cg...Cg = 3.611(2) Å, Fig. S1 and S2, ESI†). To perform the topological classification of **1**, its 2D metal-organic network has been simplified by adopting the concept of the simplified underlying net,^{15,16} namely, by omitting the terminal phenyl ligands and contracting the μ_4 -L³⁻ and μ_3 -OH⁻ nodes to their centroids. The resulting binodal 3,4-connected layer (Fig. 1d) is built from the 3-connected topologically similar Cd1 and μ_3 -OH⁻ nodes, as well as the 4-connected Cd2 and μ_4 -L³⁻ nodes that are also topologically equivalent. This layer reveals a rather rare **3,4L33** topology¹⁴ with the point symbol of (4².6)(4³.6².8), wherein the (4².6) and (4³.6².8) indices correspond to the pairs of Cd1/ μ_3 -OH⁻ and Cd2/ μ_4 -L³⁻ nodes, respectively. Further simplification of this underlying net by treating the tetracadmium(II) [Cd₄(μ_3 -OH)₂]⁶⁺ blocks as the 6-connected cluster nodes gives rise to a binodal 3,6-connected layer with the **kgd** [Shubnikov plane net (3.6.3.6)/dual] topology.^{15,16} It is defined by the point symbol of (4³)₂(4⁶.6⁶.8³), with the (4³) and (4⁶.6⁶.8³) notations corresponding to the

3-connected μ_4 -L and 6-connected $[\text{Cd}_4(\mu_3\text{-OH})_2]^{6+}$ nodes, respectively.



Scheme 3 Various coordination modes for L^{3-} , bpdC^{2-} , H_2biim , and Hbiim^- in compounds 1–6.



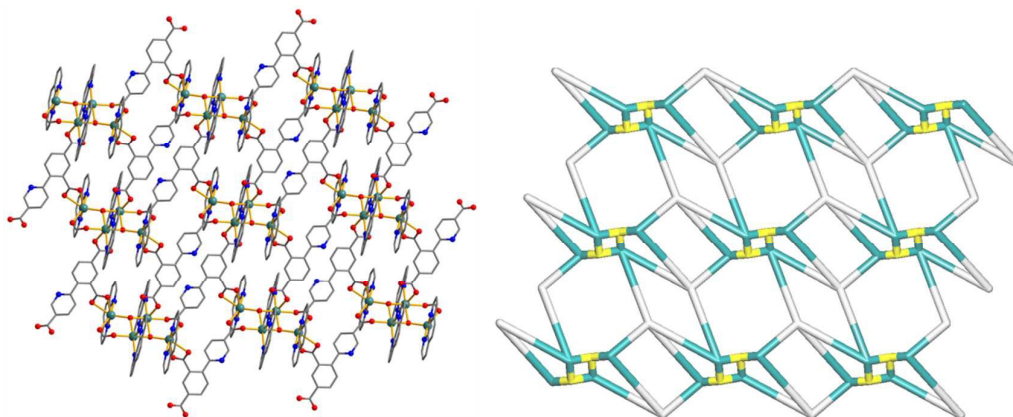


Fig. 1 Structural fragments of **1**. (a) The coordination environment of the Cd(II) ions. The hydrogen atoms are omitted for clarity. Symmetry codes: i = $-x + 1, -y + 2, -z + 1$; ii = $-x, -y + 2, -z$; iii = $x, y + 1, z$. (b) Tetracadmium(II) unit. Symmetry code: i = $-x, -y + 2, -z$. (c) View of the 2D layer along the bc plane. (d) Topological representation of the underlying 2D binodal 3,4-connected layer with the **3,4L33** topology. Color codes: Cd1 and Cd2 atoms (turquoise), centroids of $\mu_3\text{-OH}^-$ nodes (yellow), centroids of $\mu_4\text{-L}^{3-}$ nodes (gray).

4.2.2 $\{[\text{Mn}_3(\mu_5\text{-L})_2(\text{phen})_2(\text{H}_2\text{O})] \cdot \text{H}_2\text{O}\}_n$ (**2**). The asymmetric unit of **2** consists of three crystallographically independent Mn(II) atoms, two $\mu_5\text{-L}^{3-}$ blocks, two phen ligands, one coordinated and one lattice water molecule. As depicted in Fig. 2a, both Mn1 and Mn3 atoms are six-coordinate and possess a distorted octahedral coordination environment. The Mn1 center is coordinated by three O atoms from three individual $\mu_5\text{-L}^{3-}$ blocks, one O atom from coordinated water molecule, and two N atoms from phen ligand. The Mn3 center is bound by four O atoms from the three different $\mu_5\text{-L}^{3-}$ ligands and two N atoms from phen moiety. The five-coordinate Mn2 center adopts a distorted square pyramidal geometry filled by five carboxylate oxygen atoms from four individual $\mu_5\text{-L}^{3-}$ ligands. The lengths of the Mn–O bonds are in the

2.053(6)–2.464(8) Å range, while the Mn–N bonds are in the 2.259(6)–2.354(5) Å interval (Table S1), being comparable to those found in some reported Mn(II) compounds.^{2d,2f,4a,4b,4g,5b} In **2**, the L³⁻ ligands exhibit a μ_5 -coordination mode (Scheme 3, mode II). The dihedral angles of 50.36 and 54.09° are observed between the pyridyl and phenyl rings in the μ_5 -L³⁻ blocks. The carboxylate groups of the μ_5 -L³⁻ moieties link the Mn(II) centers to form two different dimanganese(II) motifs with the Mn–Mn separations of 3.898(2) and 4.116(2) Å (Fig. 2b). These Mn₂ units are multiply interlinked by other COO⁻ groups of the L³⁻ blocks to form a 3D metal-organic framework (Fig. 2c, Fig. S3 and S4, ESI†). From the topological viewpoint, this framework is very complex due to the presence of three different Mn centers and two types of μ_5 -L³⁻ blocks. An underlying net of **2** (Fig. 2c) has been generated after omitting the terminal phen and H₂O moieties, and contracting the μ_5 -L³⁻ blocks to the respective centroids. The resulting tetranodal 3,4,5,5-connected net is topologically unique and can be defined by the point symbol of (4².6⁴)(4².6)₂(4³.6³.8⁴)(4³.6⁶.8), in which the (4².6⁴), (4².6), (4³.6³.8⁴), and (4³.6⁶.8) indices are those of the 4-connected Mn₂, 3-connected Mn₁ and Mn₃, and two 5-connected μ_5 -L³⁻ nodes, respectively. An unprecedented character of this topology has been confirmed by a search of different databases.^{15–17}

(a)**(b)**

two crystallographically unique Cd(II) ions, one $\mu_3\text{-L}^{3-}$ block, two terminal H_2biim ligands, and one $\mu_2\text{-Hbiim}^-$ linker. Both six-coordinate Cd1 and Cd2 atoms show a distorted octahedral environment (Fig. 3a). The Cd1 center is coordinated by one O and N atom from the same $\mu_3\text{-L}^{3-}$ block, two N atoms from one H_2biim moiety, and two N atoms from one $\mu_2\text{-Hbiim}^-$ ligand. The Cd2 center is bound by three O atoms from two $\mu_3\text{-L}^{3-}$ blocks, two N atoms from one H_2biim moiety, and one N atom from $\mu_2\text{-Hbiim}^-$ ligand. The lengths of the Cd–O bonds range from 2.212(5) to 2.528(6) Å, whereas the Cd–N bonds vary from 2.291(6) to 2.485(6) Å; these bonding parameters lie within the typical values observed in various related cadmium(II) derivatives.^{2b,3b,4b,5c,11,17} In **3**, the L^{3-} block shows a μ_3 -coordination mode (Scheme 3, mode III), in which the carboxylate groups act in the monodentate or bidentate modes. The dihedral angle between the pyridyl and phenyl rings in L^{3-} is 65.88°. The H_2biim ligands take a bidentate chelating mode (Scheme 3, mode IX). The dihedral angles of two imidazole groups are 2.07 and 9.71°. The Hbiim^- ligand adopts the μ_2 -bridging mode (Scheme 3, mode X), and has the dihedral angle between two imidazole rings of 3.57°. The $\mu_3\text{-L}^{3-}$ blocks and $\mu_2\text{-Hbiim}^-$ ligands alternately link the adjacent Cd(II) centers to form a 2D metal-organic sheet (Fig. 3b). The neighboring sheets are assembled into a 3D supramolecular framework through N–H···O hydrogen bonds (Table S2 and Fig. S5, ESI†). For the sake of topological classification, a 2D metal-organic network of **3** was simplified, namely, by reducing the $\mu_2\text{-Hbiim}^-$ and $\mu_3\text{-L}^{3-}$ nodes to their centroids and eliminating the terminal H_2biim moieties.^{15,18} The obtained underlying net (Fig. 3c) is assembled from the 3-connected Cd2 and $\mu_3\text{-L}^{3-}$

nodes (topologically equivalent), as well as the 2-connected Cd1 atoms and μ_2 -Hbiim⁻ linkers. Its topological analysis discloses a uninodal 3-connected 2D double layer with the **fes** [Shubnikov plane net (4.8²)] topology.^{15,16,18}

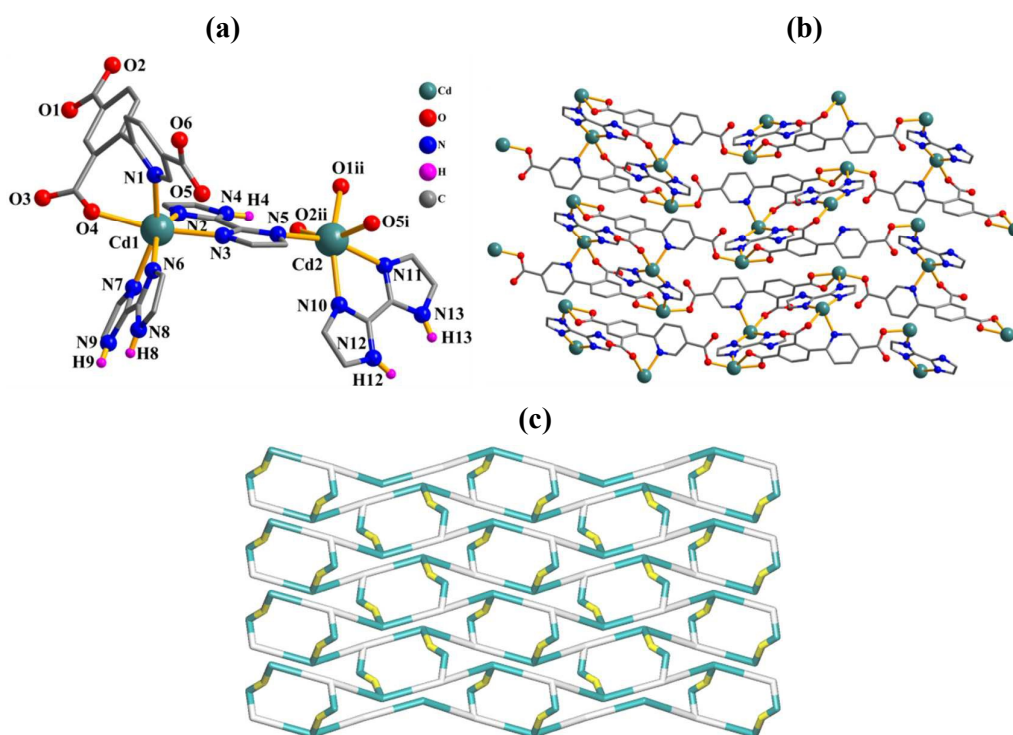
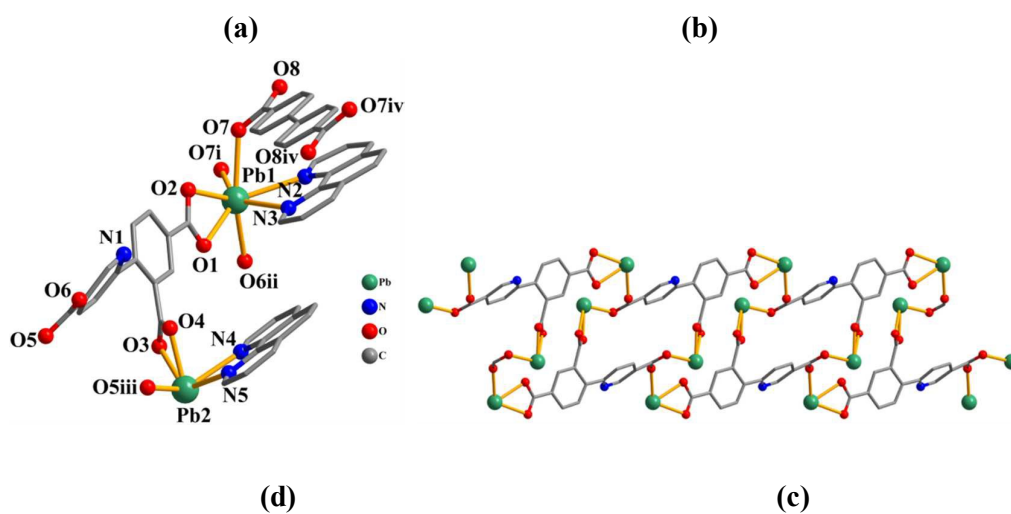


Fig. 3 Structural fragments of **3**. (a) The coordination environment of the Cd(II) ions in **3**. The hydrogen atoms are omitted for clarity except ones bond to nitrogen atoms of the H₂biim and Hbiim⁻ ligands. Symmetry codes: i = $-x, y - 1/2, -z + 1/2$; ii = $-x + 1/2, -y + 1/2, -z + 1/2$. (b) A perspective of 2D layer along the *ab* plane. The H₂biim ligands are omitted for clarity. (c) Topological representation of the underlying 2D metal-organic network in **3** showing a uninodal 3-connected layer with the **fes** topology; view along the *c* axis. Color codes: 2- and 3-connected Cd1 and Cd2 atoms (turquoise), centroids of 3-connected μ_3 -L³⁻ nodes (gray), centroids of 2-connected

μ_2 -Hbiim⁻ linkers (yellow).

4.2.4 $\{[\text{Pb}_2(\mu_4\text{-L})(\mu_4\text{-bpdC})_{0.5}(\text{phen})_2]\cdot\text{H}_2\text{O}\}_n$ (**4**). The asymmetric unit of **4** contains two crystallographically unique Pb(II) ions, one $\mu_4\text{-L}^{3-}$ block, a half of $\mu_4\text{-bpdC}^{2-}$ spacer, two phen moieties, and one lattice water molecule. As shown in Fig. 4a, the Pb1 atom is seven-coordinate and adopts a distorted pentagonal bipyramidal geometry formed by three O atoms from the two different $\mu_4\text{-L}^{3-}$ blocks, two O atoms from two distinct $\mu_4\text{-bpdC}^{2-}$ ligands, and two N atoms from the phen moiety. The five-coordinate Pb2 center is surrounded by three O atoms from the two individual $\mu_4\text{-L}^{3-}$ blocks and two N atoms from the phen ligand, leading to a distorted trigonal bipyramidal geometry. The Pb–O distances range from 2.350(6) to 2.666(6) Å, whereas the Pb–N distances vary from 2.553(7) to 2.800(7) Å (Table S1). Although some of these distances are somewhat elongated, they are still well below the sum of the Van der Waals radii for Pb and O [3.54 Å] or Pb and N [3.57 Å] atoms,¹⁷ and are also comparable with the bond lengths observed in other Pb(II) compounds.^{2b,4b,19} In addition, there are some weak Pb–O interactions in the range of 2.853(7)–3.460(7) Å which, if considered, would allow to describe both Pb1 and Pb2 centers as eight-coordinate. In **4**, the L^{3-} block shows a μ_4 -coordination mode (Scheme 3, mode IV). The dihedral angle between the pyridyl and phenyl rings in the L^{3-} is 53.72°. The bpdC^{2-} ligand also takes a μ_4 -coordination mode (Scheme 3, mode V), in which the two carboxylate groups show a μ_2 -bridging tridentate mode. The $\mu_4\text{-L}^{3-}$ blocks alternately link the adjacent Pb(II) centers to form the 1D chain motifs (Fig. 4b). Such neighboring motifs are pillared by the $\mu_4\text{-bpdC}^{2-}$ ligands to form a 3D framework (Fig.

4c). The presence of two different Pb centers and two structurally distinct and multiply bridging polycarboxylate ligands in **4** explains a very complex architecture of its 3D metal-organic framework. Hence, to better understand the structure of **4**, we have generated an underlying net and carried out its topological analysis. A simplified net (Fig. 4d) has been obtained after reducing the μ_4 -L³⁻ and μ_4 -bpdC²⁻ blocks to their centroids and eliminating the terminal phen moieties. The obtained trinodal 3,4,4-connected 3D framework is composed of the 4-connected Pb1 and μ_4 -bpdC²⁻ nodes (topologically distinct), 3-connected μ_4 -L³⁻ nodes (these have mutually common edges), and 2-connected Pb2 atoms. This net reveals an unreported topology that is described by the point symbol of $(4.6.8^4)_2(4^2.8^4)(6^2.8)_2$, wherein the $(4.6.8^4)$, $(4^2.8^4)$, and $(6^2.8)$ indices are those of the Pb1, μ_4 -bpdC²⁻, and μ_4 -L³⁻ nodes, respectively. The novelty of this topological type has been confirmed by a search of different databases.¹⁵⁻¹⁷



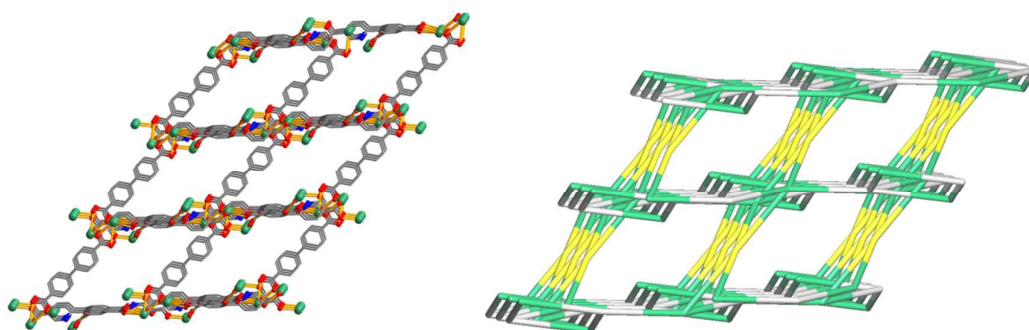


Fig. 4 Structural fragments of **4**. (a) The coordination environment of the Pb(II) ions. The hydrogen atoms are omitted for clarity. Symmetry codes: i = $-x + 2, -y + 1, -z$; ii = $x + 1, y, z - 1$; iii = $-x, -y, -z + 2$; iv = $x - 1, y, z + 1$. (b) 1D chain motif along the c axis. The phen ligands are omitted for clarity. (c) A perspective of 3D metal-organic framework along the b axis. The phen ligands are omitted for clarity. (d) Topological representation of the underlying 3D metal-organic framework in **4** showing a topologically unique trinodal 3,4,4-connected net defined by the point symbol of $(4.6.8^4)_2(4^2.8^4)(6^2.8)_2$; view along the b axis. Color codes: 4-connected Pb1 and 2-connected Pb2 atoms (green), centroids of 3-connected $\mu_4\text{-L}^{3-}$ nodes (gray), centroids of 4-connected $\mu_4\text{-bpdc}^{2-}$ nodes (yellow).

4.2.5 $[\text{Cd}_2(\mu_5\text{-L})(\mu_2\text{-bpdc})_{0.5}(\text{phen})_2]_n$ (**5**). As shown in Fig. 5a, the asymmetric unit of **5** consists of two crystallographically unique Cd(II) ions, one $\mu_5\text{-L}^{3-}$ block, a half of $\mu_2\text{-bpdc}^{2-}$ ligand, and two phen moieties. Both Cd1 and Cd2 atoms possess a distorted octahedral coordination environment. The Cd1 center is coordinated by two O atoms from two different $\mu_5\text{-L}^{3-}$ blocks, two O atoms from one $\mu_2\text{-bpdc}^{2-}$ moiety, and two N atoms from one phen ligand. The Cd2 center is bound by four O atoms from three individual $\mu_5\text{-L}^{3-}$ blocks and two N atoms from one phen ligand. The lengths of Cd–O bonds range from 2.233(4) to 2.533(3) Å, while the Cd–N bonds vary from 2.319(5) to 2.381(4) Å. All the Cd–O and Cd–N distances in **1**, **3**, and **5** (Table S1) are comparable to those in other reported Cd(II)

compounds.^{2b,2h,3b,3d,4a,4b,5c,11,17,20} In **5**, the L^{3-} block shows a μ_5 -coordination mode (Scheme 3, mode VI), in which the three carboxylate groups adopt the terminal bidentate or μ_2 -bridging bidentate and tridentate modes. The dihedral angle between the pyridyl and phenyl rings in L^{3-} is 25.38° . The $bpdc^{2-}$ ligand acts as a μ_2 -linker (Scheme 3, mode VII). The μ_5-L^{3-} blocks alternately link the adjacent Cd(II) centers to form a 1D chain motif (Fig. 5b). These neighboring motifs are interconnected by the μ_2 - $bpdc^{2-}$ linkers to generate a 2D metal-organic network (Fig. 5c). It is further extended into a 3D supramolecular framework via the weak C–H \cdots O hydrogen bond interactions (Figs. S6 and S7, ESI \dagger). To get further insight into an intricate 2D metal-organic network of **5**, we have performed its topological analysis.^{14,17} An underlying net has been generated by omitting the terminal phen ligands and reducing the μ_5-L^{3-} and μ_2 - $bpdc^{2-}$ blocks to their centroids. The resulting trinodal 3,3,5-connected 2D layer (Fig. 5d) is composed of the 3-connected topologically distinct Cd1 and Cd2 nodes, 5-connected μ_5-L^{3-} nodes, and 2-connected μ_2 - $bpdc^{2-}$ linkers. This layer features a unique topology¹⁴ that can be defined by the point symbol of $(4.6^2)(4^3)(4^4.6^4.8^2)$, wherein the (4.6^2) , (4^3) , and $(4^4.6^4.8^2)$ notations are those of the Cd1, Cd2, and μ_5-L^{3-} nodes respectively. Further simplification of this layer by treating the $[Cd_2(\mu_2-bpdc)]^{2+}$ blocks (these are based on the Cd1 atoms) as the 4-connected cluster nodes leads to a trinodal 3,4,5-connected net with a rare **3,4,5L5** topology and point symbol of $(4^3)_2(4^4.6^2)(4^5.6^5)_2$ (Fig. 5e).¹⁵

(a)

(b)

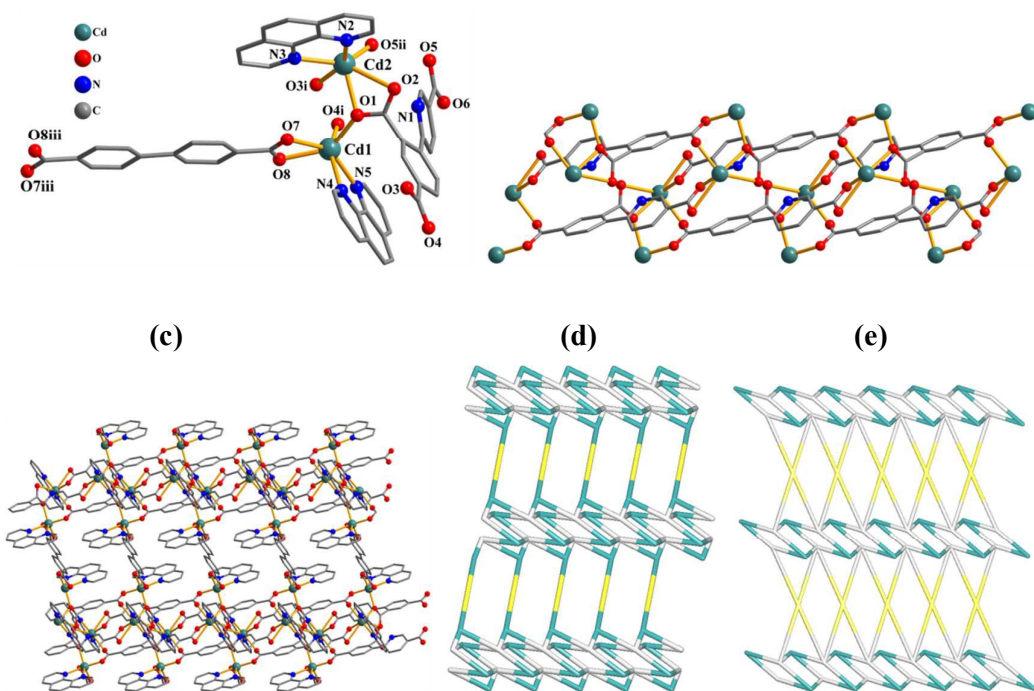


Fig. 5 Structural fragments of **5**. (a) The coordination environment of the Cd(II) ions. The hydrogen atoms are omitted for clarity. Symmetry codes: i = $x + 1, y, z$; ii = $-x + 2, -y + 2, -z$; iii = $-x + 2, -y + 1, -z + 1$. (b) 1D chain motif along the b axis. The phen ligands are omitted for clarity. (c) A perspective of 2D metal-organic network along the b axis. (d, e) Topological representations of the underlying 2D metal-organic networks in **5** showing: (d) topologically unique trinodal 3,3,5-connected layer with the point symbol of $(4.6^2)(4^3)(4^4.6^4.8^2)$, and (e) further simplified trinodal 3,4,5-connected layer with the **3,4,5L5** topology after treating $[\text{Cd}_2(\mu_2\text{-bpdc})]^{2+}$ blocks (composed of Cd1 atoms) as cluster nodes; (d, e) rotated views along the b axis. Color codes: (d) 3-connected Cd1 and Cd2 nodes (turquoise), centroids of 5-connected $\mu_5\text{-L}^{3-}$ nodes (gray), centroids of 2-connected $\mu_2\text{-bpdc}^{2-}$ linkers (yellow); (e) 3-connected Cd2 nodes (turquoise), centroids of 4-connected $[\text{Cd}_2(\mu_2\text{-bpdc})]^{2+}$ cluster nodes (yellow), centroids of 5-connected $\mu_5\text{-L}$ nodes (gray).

4.2.6 [Zn₂(μ₄-L)(μ₂-bpdc)_{0.5}(py)₂]_n (6**).** In the asymmetric unit of **6**, there are two crystallographically unique Zn(II) ions, one μ₄-L³⁻ block, a half of μ₂-bpdc²⁻ ligand, and two pyridine moieties. As shown in Fig. 6a, the five-coordinate Zn1 atom is surrounded by four O and one N atoms from three individual μ₄-L³⁻ blocks, thus constructing a distorted square pyramidal environment. The Zn2 atom is six-coordinated by two O atoms from one μ₄-L³⁻ block, two O atoms from one μ₂-bpdc²⁻ ligand, and two N atoms from py moieties, forming a distorted octahedral geometry. The Zn–O bond lengths range from 1.935(5) to 2.412(7) Å, whereas the Zn–N distances vary from 2.037(6) to 2.065(6) Å (Table S1), which are in good agreement with those reported for other Zn(II) derivatives.^{3c,4e,4g,11,17} In **6**, the L³⁻ block acts as a μ₄-spacer (Scheme 3, mode VIII), in which the carboxylate groups adopt the terminal bidentate and μ₂-bridging tridentate modes, respectively. The dihedral angle between the pyridyl and phenyl rings in the L³⁻ is 47.70°. The bpdc²⁻ ligand takes the same μ₂-coordination mode (Scheme 3, mode VII) as that in **5**. The carboxylate O and pyridyl N atoms of the μ₄-L³⁻ ligands bridge the adjacent Zn(II) ions to form a 2D sheet motif (Fig. 6b). These motifs are further assembled into a 3D metal-organic framework by the linkage of μ₂-bpdc²⁻ blocks with Zn(II) ions (Fig. 6c). A 3D metal-organic framework of **6** has been simplified for the sake of topological classification.¹⁵ Thus, the terminal py ligands have been omitted, whereas the bridging μ₂-bpdc²⁻ and μ₄-L³⁻ moieties have been contracted to their centroids, resulting in an underlying 3D net (Fig. 6d). From the topological viewpoint, this net can be classified as a binodal 3,4-connected framework with the **ins** (InS) topology.^{15,16,18} It is defined

by the point symbol of $(6^3)(6^5.8)$, with the (6^3) and $(6^5.8)$ notations corresponding to the 3-connected Zn1 and 4-connected $\mu_4\text{-L}^{3-}$ nodes, respectively. In this net, the Zn2 atoms and $\mu_2\text{-bpd}c^{2-}$ blocks act as the 2-connected linkers.

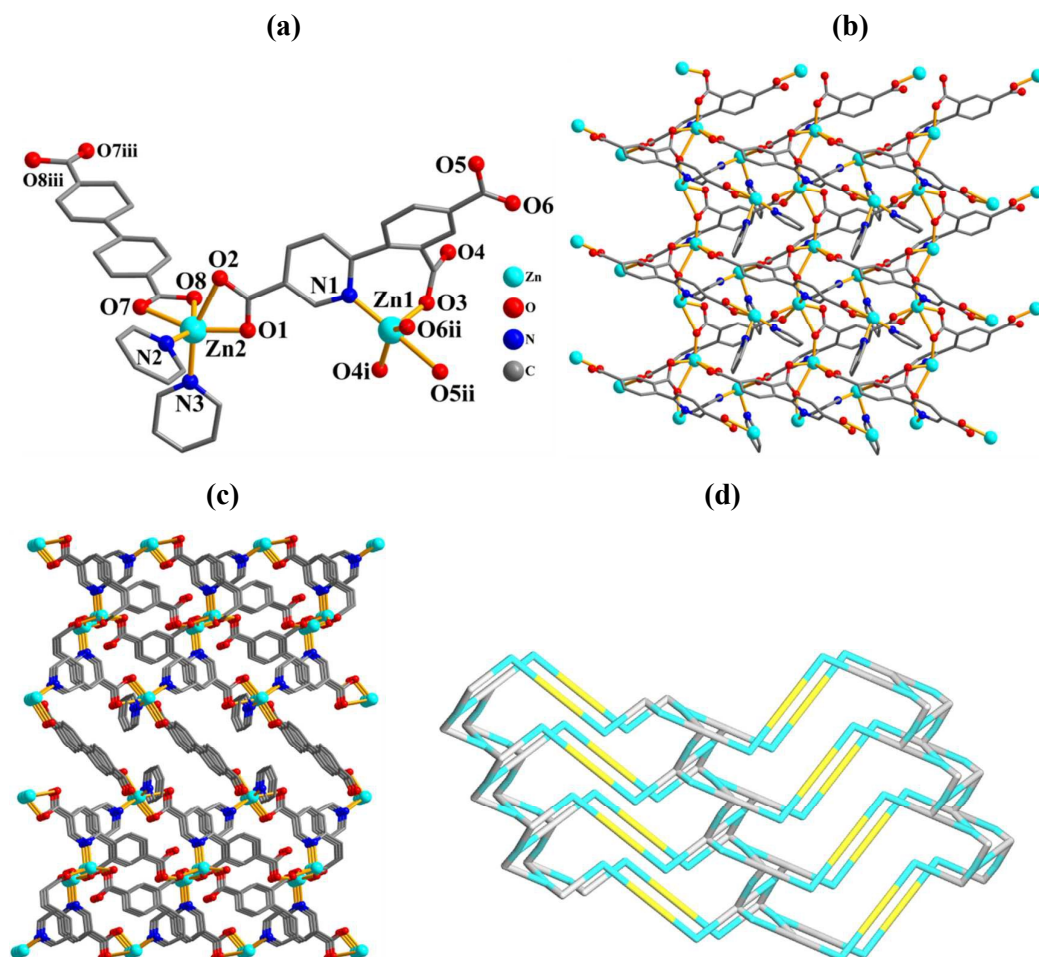


Fig. 6 Structural fragments of **6**. (a) The coordination environment of the Zn(II) ions. The hydrogen atoms are omitted. Symmetry codes: i = $-x + 2, y + 1/2, -z + 1/2$; ii = $-x + 1, y + 1/2, -z + 1/2$; iii = $-x - 1, -y + 1, -z$. (b) View of the 2D layer motif along the *ab* plane. (c) A perspective of 3D metal-organic framework along the *b* axis. (d) Topological representation of the underlying 3D metal-organic framework showing a binodal 3,4-connected net with the **ins** topology; view along the *a* axis. Color codes: 2- and 3-connected Zn2 and Zn1 atoms (cyan), centroids of 4-connected $\mu_4\text{-L}^{3-}$ nodes

(gray), centroids of 2-connected μ_2 -bpdc²⁻ linkers (yellow).

4.2.7 Diverse coordination modes of L³⁻ and structural comparison. As shown in Scheme 3, the 4-(5-carboxypyridin-2-yl)isophthalate ligand exhibits versatile coordination modes in products **1–6** acting as a μ_3 -, μ_4 -, or μ_5 -L³⁻ building block, in which three carboxylate groups can adopt one of the following four coordination modes: monodentate, terminal and μ_2 -bridging bidentate, and μ_2 -bridging tridentate. Besides, the N atom of the pyridine functionality of L³⁻ also acts as a N-donor in the Cd(II) and Zn(II) derivatives **3** and **6**, respectively. In polymer **3**, the H₂biim ligand takes a bidentate chelating mode whereas the Hbiim⁻ moiety adopts the μ_2 -bridging mode. In compound **4**, the bpdc²⁻ ligand acts as a μ_4 -spacer with both carboxylate groups exhibiting a μ_2 -bridging tridentate mode. In **5** and **6**, the bpdc²⁻ ligand behaves as a μ_2 -pillar. A notable feature of L³⁻ consists of the rotation of the C–C single bond between the pyridyl and phenyl rings (the dihedral angles are in the 25.38–65.88° range), thus fulfilling the requirement of coordination geometries of metal ions during the self-assembly process. The obtained results indicate that the L³⁻ blocks can adopt a diversity of coordination modes to bind the metal centers in the compounds **1–6**. Products **1** and **2** were synthesized under the same reaction conditions, except for the type of metal chloride used (CdCl₂·H₂O for **1** and MnCl₂·4H₂O for **2**). Their structural differences indicate that the assembly process is metal ion-dependent, thus resulting in a 2D layer structure in **1** and a 3D metal-organic framework in **2**. The structural differences between the lead and cadmium containing coordination polymers **4** and **5** can be attributed to the same reason. The distinct structural type of the compounds **1**

and **3** was caused by the introduction of different auxiliary ligands (phen for **1** and H₂bim for **3**), under the same reaction conditions. All these observations indicate that the type of the metal ions and auxiliary ligands have significant effects on the formation and structures of the resulting coordination polymers.

4.3 Thermal analysis and PXRD results

Powder X-ray diffraction experiments were carried out for compounds **1–6**. The patterns for the as-synthesized bulk materials closely match the simulated ones from the single crystal X-ray diffraction data (Fig. S8, ESI†), thus indicating the phase purity of the crystalline samples. To determine the thermal stability of **1–6**, their thermal behavior was investigated under nitrogen atmosphere by TGA (Fig. S9, ESI†). Compound **1** lost its two lattice water molecules (exptl, 3.6%; calcd, 3.9%) from 55 to 105 °C, and then the decomposition occurs at 315 °C. For **2**, there is one distinct weight loss effect in the 56–125 °C range, corresponding to the release of one lattice water molecule and one H₂O ligand (exptl, 3.4%; calcd, 3.2%). The decomposition of the remaining solid begins at 335 °C. The TGA curves of compounds **3**, **5**, and **6** show that there is no appreciable weight change up to 330, 295, and 285 °C, respectively, while further heating of the samples leads to their decomposition. For compound **4**, the weight loss corresponding to the release of one lattice water molecule was observed from 69 to 116 °C (exptl, 1.4%; calcd, 1.5%), and the decomposition of the dehydrated solid begins at 253 °C. We suppose that the final decomposition products of compounds **1–6** can be the corresponding metal oxides (e.g., CdO for **1**, **3**, and **5**),

although a more prolonged heating would be required in some cases to achieve a full decomposition of the samples.

4.4 Luminescent properties

The emission spectra of H₃L, H₂bpdc, and compounds **1** and **3–6** were measured in the solid-state at room temperature and are given in Fig. 7. The “free” H₃L and H₂bpdc ligands display weak photoluminescence with an emission maximum at 473 and 407 nm if excited at 380 and 335 nm, which may be attributed to the $\pi^* \rightarrow n$ or $\pi^* \rightarrow \pi$ transitions.^{19,21–29} For compounds **1** and **3–6**, the emission bands of higher (**4**, **6**) or significantly higher (**1**, **3**, **5**) intensity are detected with the maximum at 415 nm ($\lambda_{\text{ex}} = 335$ nm) for **1**, 525 nm ($\lambda_{\text{ex}} = 380$ nm) for **3**, 580 nm ($\lambda_{\text{ex}} = 392$ nm) for **4**, 469 nm ($\lambda_{\text{ex}} = 376$ nm) for **5**, and 423 nm ($\lambda_{\text{ex}} = 338$ nm) for **6**. The emission bands of compounds **1**, **5**, and **6** were blue-shifted by 58, 4, and 50 nm compared with the “free” H₃L. In contrast, the emission bands of compounds **3** and **4** were red-shifted by 52 and 107 nm relatively to H₃L. If compared with the “free” H₂bpdc, the emission maxima of mixed-ligand derivatives **4**, **5**, and **6** are red-shifted by 173, 62, and 16 nm, respectively. The observed emission bands cannot be ascribed to the LMCT or MLCT processes. Thus, the intraligand and ligand-to-ligand charge transitions are probably responsible for the emission properties of the compounds **1** and **3–6**.^{21–29} The enhancement of luminescence in the compounds in comparison with H₃L can be attributed to the binding of ligands to the metal centers, which can effectively increase the rigidity of the ligand and reduce the loss of energy by radiationless decay.^{22–29}

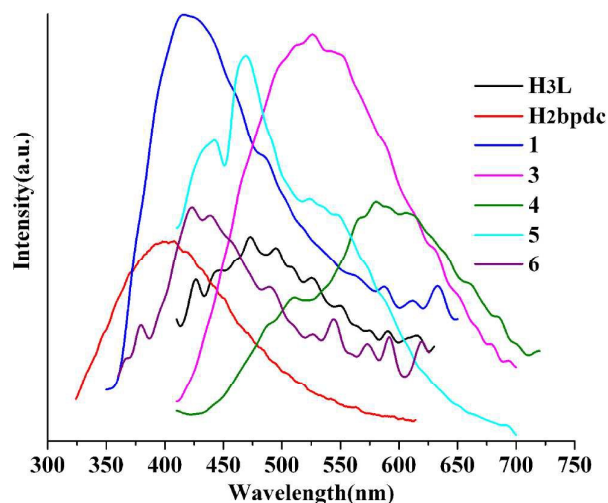


Fig. 7 Solid state emission spectra of H₃L, H₂bpdc, and compounds **1** and **3–6** at room temperature.

4.5 Magnetic properties

Variable-temperature magnetic susceptibility studies were carried out in the 2–300 K temperature range using a powder sample of compound **2**. As shown in Fig. 8, the $\chi_M T$ value at 300 K is $12.97 \text{ cm}^3 \cdot \text{mol}^{-1} \cdot \text{K}$, which is close to that of $13.12 \text{ cm}^3 \cdot \text{mol}^{-1} \cdot \text{K}$ expected for three magnetically isolated high-spin Mn(II) centers ($S_{\text{Mn}} = 5/2$, $g = 2.0$). The $\chi_M T$ values steadily decrease on lowering the temperature and reach the minimum of $2.21 \text{ cm}^3 \cdot \text{mol}^{-1} \cdot \text{K}$ at 2.00 K. Between 2 and 300 K, the magnetic susceptibility can be fitted to the Curie–Weiss law with $C = 13.30 \text{ cm}^3 \cdot \text{mol}^{-1} \cdot \text{K}$ and $\theta = -7.58 \text{ K}$. These results indicate an antiferromagnetic interaction between the adjacent Mn(II) ions. According to the crystal structure of **2**, there are two sets of magnetic exchange pathways: one is through carboxylate bridges within the two different dimers, the other one is inter-dimers through

carboxylate bridges or L^{3-} blocks (Fig. S3 and S4, ESI†). Because of the long inter-dimers Mn–Mn distances (intra- and inter-dimers superexchange distances are 3.898(2)–4.116(2) and 4.902(2)–9.176(2) Å, respectively), it is expected that the intra-dimers interactions in compound **2** are much stronger than the inter-dimers coupling and should dominate its magnetic behavior.

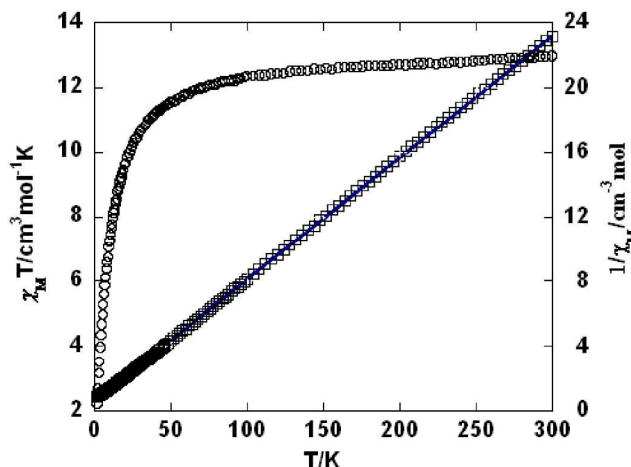


Fig. 8 Temperature dependence of $\chi_M T$ (O) and $1/\chi_M$ (□) vs. T for compound **2**. The blue line shows the Curie-Weiss fitting.

5. Conclusions

In this work, we have opened up the application of 4-(5-carboxypyridin-2-yl)isophthalic acid (H_3L) as a novel versatile tricarboxylate building block with a pyridine functionality for the design of various mixed-ligand 2D coordination polymers or 3D metal-organic frameworks. Hence, a new series of Cd(II), Mn(II), Pb(II), and Zn(II) coordination polymers has been generated by hydrothermal self-assembly reactions, using different metal(II) chlorides as a metal source, H_3L as an unexplored principal building block, along with various auxiliary ligands. Network dimensionality, structural and topological characteristics of the

obtained products depend on the nature of the metal center and the combination of auxiliary ligands. All products have been topologically classified, disclosing the **kgd** (in **1**), **fes** (in **3**), **3,4,5L5** (in **5**), and **ins** (in **6**) topologies. Besides, topologically unique multinodal nets have been found in the very complex 3D frameworks of **2** and **4**, thus contributing to the identification of novel topological types in MOFs. Further research toward exploring H₃L and related pyridine polycarboxylate building blocks for the design of functional coordination polymers will be pursued.

Electronic supporting information (ESI) available

Selected bond distances and angles (Table S1), hydrogen bonding parameters (Table S2), additional structural representations (Fig. S1–S7), PXRD patterns (Fig. S8) and TGA curves (Fig. S9) of the compounds **1–6**, as well as crystallographic data in CIF format (CCDC 1402748–1402753).

Acknowledgements

This work was financially supported by the National Natural Science Foundation of China (Project 21201091) and the Fundamental Research Funds for the Central Universities (Project lzujbky-2013-59). AMK acknowledges the Foundation for Science and Technology (FCT), Portugal (PTDC/QUI-QUI/121526/2010, PEst-OE/QUI/UI0100/2013).

References

- 1 (a) W. X. Zhang, P. Q. Liao, R. B. Lin, Y. S. Wei, M. H. Zeng and X. M. Chen, *Coord. Chem. Rev.*, 2015, **293–294**, 263–278; (b) Q. L. Zhu and O. Xu, *Chem. Soc. Rev.*, 2014, **43**, 5468–5512; (c) X. D. Zheng and T. B. Lu, *CrystEngComm*, 2010, **12**, 324–336; (d) G. Férey, *Chem. Soc. Rev.*, 2008, **37**, 191–214; (e) Z. Q. Wang and S. M. Cohen, *Chem. Soc. Rev.*, 2009, **38**, 1315–1329; (f) J. R. Li, R. J. Kuppler and H. C. Zhou, *Chem. Soc. Rev.*, 2009, **38**, 1477–1504; (g) G. Férey and C. Serre, *Chem. Soc. Rev.*, 2009, **38**, 1380–1399; (h) Q. W. Li, W. Y. Zhang, O. S. Miljanic, C. H. Sue, Y. L. Zhao, L. H. Li, C. B. Knobler, J. Fraser Stoddart and O. M. Yaghi, *Science*, 2009, **325**, 855–859; (i) J. Y. Lee, O. K. Farha, J. Roberts, K. A. Scheidt, S. T. Nguyen and J. T. Hupp, *Chem. Soc. Rev.*, 2009, **38**, 1450–1459; (j) L. Q. Ma, C. Abney and W. B. Lin, *Chem. Soc. Rev.*, 2009, **38**, 1248–1256; (k) Y. B. He, O. Keeffe and B. L. Chen, *Chem. Soc. Rev.*, 2014, **43**, 5618–5656.
- 2 (a) L. N. Zhang, C. Zhang, B. Zhang, C. X. Du and H. W. Hou, *CrystEngComm*, 2015, **17**, 2837–2846; (b) X. X. Xu, Y. Lu, E. B. Wang, Y. Ma and X. L. Bai, *Cryst. Growth Des.*, 2006, **6**, 2029–2035; (c) M. Du, C. P. Li, C. S. Liu and S. M. Fang, *Coord. Chem. Rev.*, 2013, **257**, 1282–1305; (d) C. Y. Niu, X. F. Zheng, X. S. Wan and H. Z. Kou, *Cryst. Growth Des.*, 2011, **11**, 2874–2888; (e) K. H. Li, W. C. Song, Y. W. Li, Y. Q. Chen and X. H. Bu, *Cryst. Growth Des.*, 2012, **12**, 1064–1068; (f) M. Chen, S. S. Chen, T. Okamura, Z. Su, M. S. Chen, Y. Zhao and W. Y. Sun, *Cryst. Growth Des.*, 2011, **11**, 1901–1912; (g) X. M. Chen and M. L. Tong, *Acc. Chem. Res.*, 2007, **40**, 162–170; (h) R. Singh and P. K. Bharatdwaj, *Cryst. Growth Des.*, 2013, **13**, 3722–

3733; (i) A. M. Stepenson and D. Ward, *Chem. Commun.*, 2012, **48**, 3605–3607.

3 (a) A. S. Munn, S. Amabilino, T. W. Stevens, L. M. Daniels, G. J. Clarkson, F. Millange, M. J. Lennox, T. Düren, S. Bourelly, P. L. Llewellyn and R. I. Walton, *Cryst. Growth Des.*, 2015, **15**, 891–899; (b) Z. J. Wang, L. Qin, X. Zhang, J. X. Chen and H. G. Zheng, *Cryst. Growth Des.*, 2015, **15**, 1303–1310; (c) J. Z. Gu, W. G. Lu, L. Jiang, H. C. Zhou and T. B. Lu, *Inorg. Chem.*, 2007, **46**, 5835–5837; (d) S. Tripathi and G. Anantharaman, *CrystEngComm*, 2015, **17**, 2754–2768; (e) J. Z. Gu, D. Y. Lv, Z. Q. Gao, J. Z. Liu, W. Dou and Y. Tang, *J. Solid State Chem.*, 2011, **184**, 675–683; (f) H. Y. Liu, H. Wu, J. Yang, Y. Y. Liu, B. Liu and J. F. Ma, *Cryst. Growth Des.*, 2011, **11**, 2920–2927; (g) Y. Zhang, Q. F. Liu, G. E. Xing and Z. Q. Zhang, *J. Mol. Struct.*, 2015, **1085**, 121–125; (h) J. L. Song, F. Y. Yi and J. G. Mao, *Cryst. Growth Des.*, 2009, **9**, 3273–3277.

4 (a) J. Z. Gu, Z. Q. Gao and Y. Tang, *Cryst. Growth Des.*, 2012, **12**, 3312–3323; (b) J. Z. Gu, A. M. Kirillov, J. Wu, D. Y. Lv, Y. Tang and J. C. Wu, *CrystEngComm*, 2013, **15**, 10287–10303; (c) B. L. Chen, N. W. Ockwig, A. R. Millward, D. S. Contreras and O. M. Yaghi, *Angew. Chem., Int. Ed.*, 2005, **44**, 4745–4749; (e) D. Tian, Y. Pang, Y. H. Zhou, L. Guan and H. Zhang, *CrystEngComm*, 2011, **13**, 957–966; (f) L. L. Wen, F. Wang, X. K. Leng, C. G. Wang, L. Y. Wang, J. M. Gong and D. F. Li, *Cryst. Growth Des.*, 2010, **10**, 2835–2838; (g) Y. Zhao, X. H. Chang, G. Z. Liu, L. F. Ma and L. Y. Wang, *Cryst. Growth Des.*, 2015, **15**, 966–974.

5 (a) R. Mohammadinasab, M. Tabatabaee, B. M. Kukovec and H. Aghaie, *Inorg. Chim. Acta*, 2013, **405**, 368–373; (b) P. J. Saines, P. T. Barton, P. Jain and A. K.

Cheetham, *CrystEngComm*, 2012, **14**, 2711–2720; (c) G. Y. Wu, Y. X. Ren, Z. Yin, F. Sun, M. H. Zeng and M. Kurmoo, *RSC Adv.*, 2014, **4**, 24183–24188; (d) C. Wang and W. B. Lin, *J. Am. Chem. Soc.*, 2011, **133**, 4232–4235.

6 D. Y. Lv, Z. Q. Gao, J. Z. Gu,; R. Ren and W. Dou, *Trans. Met. Chem.*, 2011, **36**, 313–318.

7 Z. Q. Gao, H. J. Li and J. Z. Gu, *Chin. J. Inorg. Chem.*, 2014, **30**, 2803–2810.

8 L. V. Tsymbal, I. L. Andriichuk, Ya. D. Lampeka and V. B. Arion, *J. Struct. Chem.*, 2014, **55**, 1466–1473.

9 H. J. Li, Z. Q. Gao and J. Z. Gu, *Chin. J. Inorg. Chem.*, 2014, **30**, 2615–2620.

10 B. B. Ding, Y. Q. Weng, Z. W. Mao, C. K. Lan, X. M. Chen and B. H. Ye, *Inorg. Chem.*, 2005, **44**, 8836–8845.

11 L. Chen, S. H. Gou and J. Q. Wang, *J. Mol. Struct.*, 2011, **991**, 149–157.

12 (a) W. Q. Zhang, J. C. Yu, Y. J. Cui, X. T. Rao, Y. Zhang and G. D. Qian, *J. Alloys Comp.*, 2013, **551**, 616–620; (b) G. Labbé, A. P. Krismanich, S. de Groot, T.

Rasmusson, M. H. Shang, M. D. R. Brown, G. I. Dmitrienko and J. G. Guillemette, *J. Inorg. Biochem.*, 2012, **112**, 49–58.

13 (a) G. M. Sheldrick, *Acta Crystallogr., Sect. A: Found. Crystallogr.*, 1990, **46**, 467–473; (b) G. M. Sheldrick, *SHELXS-97*, A Program for X-ray Crystal Structure Solution, and *SHELXL-97*, A Program for X-ray Structure Refinement, Göttingen University, Germany, 1997.

14 P. van der Sluis and A. L. Spek, *Acta Crystallogr., Sect. A* 1990, **46**, 194–201.

15 (a) V. A. Blatov, *IUCr CompComm Newsletter*, 2006, **7**, 4–38; (b) V. A. Blatov, A.

- P. Shevchenko and D. M. Proserpio, *Cryst. Growth Des.*, 2014, **14**, 3576–3586.
- 16 The Reticular Chemistry Structure Resource (RCSR) Database; M. O’Keeffe, M. A. Peskov, S. J. Ramsden and O. M. Yaghi, *Acc. Chem. Res.*, 2008, **30**, 1782–1789.
- 17 See the Cambridge Structural Database (CSD, version 5.36, 2015): F. H. Allen, *Acta Crystallogr., Sect. B* 2002, **58**, 380–388.
- 18 (a) M. O’Keeffe and O. M. Yaghi, *Chem. Rev.*, 2012, **112**, 675–702; (b) M. Li, D. Li, M. O’Keeffe and O. M. Yaghi, *Chem. Rev.*, 2014, **114**, 1343–1370.
- 19 D. S. Deng,; L. L. Liu, B. M. Ji, G. J. Yin and C. X. Du, *Cryst. Growth Des.*, 2012, **12**, 5338–5348.
- 20 Y. H. Cui, J. Wu,; A. M. Kirillov, J. Z. Gu and W. Dou, *RSC Adv.*, 2015, **5**, 10400–10411.
- 21 X. R. Hao, X. L. Wang, Z. M. Su, K. Z. Shao, Y. H. Zhao, Y. Q. Lan and Y. M. Fu, *Dalton Trans.*, 2009, 8562–8566.
- 22 G. L. Xu and F. Guo, *Inorg. Chem. Commun.* 2013, **27**, 146–148.
- 23 T. Li, F. L. Wang, S. T. Wu, X. H. Huang, S. M. Chen and C. C. Huang, *Cryst. Growth Des.*, 2013, **13**, 3271–3274.
- 24 D. Sun, Z. H. Yan, V. A. Blatov, L. Wang and D. F. Sun, *Cryst. Growth Des.*, 2013, **13**, 1277–1289.
- 25 D. M. Chen, X. Z. Ma, W. Shi and P. Cheng, *Cryst. Growth Des.*, 2015, **15**, 3999–4004.
- 26 S. L. Wang, F. L. Hu, J. Y. Zhou, Y. Zhou, Q. Huang and J. P. Lang, *Cryst. Growth Des.*, 2015, **15**, 4087–4097.

27 K. Tomar, R. Rajak, S. Sanda and S. Konar, *Cryst. Growth Des.*, 2015, **15**, 2732–2741.

28 D. Sun, L. L. Han, S. Yuan, Y. K. Deng, M. Z. Xu and D. F. Sun, *Cryst. Growth Des.*, 2013, **13**, 377–385.

29 Y. Zhang, B. B. Guo, L. Li, S. F. Liu and G. Li, *Cryst. Growth Des.*, 2013, **13**, 367–376

Table 1 Crystal data and structure refinement for the compounds 1–6

Compound	1	2	3	4	5	6
Empirical formula	C ₃₈ H ₂₇ Cd ₂ N ₅	C ₅₂ H ₃₂ Mn ₃ N ₆	C ₃₂ H ₂₃ Cd ₂ N ₁₃	C ₄₅ H ₂₉ Pb ₂ N ₅	C ₄₅ H ₂₇ Cd ₂ N ₅	C ₃₁ H ₂₀ Zn ₂ N ₃
Formula weight	922.45	1129.66	910.43	1198.11	990.52	693.24
Crystal system	Triclinic	Monoclinic	Monoclinic	Triclinic	Triclinic	Monoclinic
Space group	P-1	P2 ₁ /n	I2/a	P-1	P-1	P2 ₁ /c
a (Å)	12.0855(6)	8.6220(4)	29.1344(11)	11.5662(5)	8.666(3)	8.7544(5)
b (Å)	12.1636(6)	39.658(3)	8.6686(3)	14.0642(12)	15.518(5)	8.4785(7)
c (Å)	13.5127(6)	13.6015(6)	31.9584(14)	14.1354(10)	15.924(6)	39.392(4)
α (°)	98.040(4)	90	90	65.656(8)	103.487(4)	90
β (°)	111.284(4)	92.600(5)	112.448(5)	66.949(5)	95.131(4)	92.684(7)
γ (°)	96.639(4)	90	90	82.089(5)	91.792(4)	90
Volume (Å ³)	1802.69(15)	4646.0(5)	7459.6(5)	1926.9(2)	2071.0(12)	2920.6(4)
Z	2	4	8	2	2	4
D _{calc} (g cm ⁻³)	1.699	1.615	1.621	2.065	1.588	1.577
M (Mo Kα) (mm ⁻¹)	1.243	0.883	1.200	8.794	1.087	1.699
F(000)	916	2292	3600	1140	948	1404
Data/restraints/paramet	6374/6/487	8216/0/680	6595/0/478	6812/42/545	7060/114/562	6046/24/386
Goodness-of-fit on F ²	1.091	1.051	1.036	1.041	1.103	1.076
Final R indices, [I > 2σ(I)]	R ₁ = 0.0333 wR ₂ = 0.0771	R ₁ = 0.0759 wR ₂ = 0.1934	R ₁ = 0.0541, wR ₂ = 0.1538	R ₁ = 0.0454 wR ₂ =	R ₁ = 0.0531 wR ₂ = 0.1593	R ₁ = 0.0928 wR ₂ = 0.2468
R indices (all data)	R ₁ = 0.0432 wR ₂ = 0.0873	R ₁ = 0.1146 wR ₂ = 0.2230	R ₁ = 0.0715 wR ₂ = 0.1725	R ₁ = 0.0617 wR ₂ =	R ₁ = 0.0648 wR ₂ = 0.1676	R ₁ = 0.1350 wR ₂ = 0.2620
CCDC No	1402752	1402753	1402749	1402750	1402748	1402751